RSC Advances

PAPER

View Article Online
View Journal | View Issue

Cite this: *RSC Adv.*, 2018, **8**, 39742

Polypyrrole–MXene coated textile-based flexible energy storage device†

Jinfeng Yan, Yanan Ma,* Chuankun Zhang, Xingxing Li, Weizhi Liu, Xinyu Yao, Shuai Yao and Shijun Luo

Recently, more and more researchers have devoted their efforts to developing flexible electrochemical energy storage devices to meet the development of portable and wearable electronics. Among them, supercapacitors (SCs) have been widely studied due to their high specific capacitance and power density. However, most flexible SCs often use traditional carbon materials and transition metal oxides as electrode materials. In this paper, we used an easy and low-cost way to fabricate a flexible supercapacitor based on a new type of two-dimensional material, transition metal carbides, nitrides, or carbonitrides (MXenes). By taking full advantage of the hydrophilicity and metal conductivity of MXene nanosheets, an extremely simple "dipping and drying" method was used to achieve conductive textile electrodes with a specific capacitance of 182.70 F g^{-1}, which is higher than reported for carbon nanotubes (CNTs) and active carbon. To further improve the capacitive performance of the MXene-based electrode and avoid the poor oxygen oxidation of MXene, polypyrrole (PPy) was electrochemically deposited on the surface of MXene textiles, thus producing a PPy–MXene coated textile electrode with a specific capacitance of 343.20 F g^{-1}. In addition, a symmetrical solid-state supercapacitor based on MXene–PPy textiles was assembled, which achieved an energy density of 1.30 mW h g^{-1} (power density = 41.1 mW g^{-1}). This work introduces a new type of MXene-based textile SC, which provides a promising candidate for flexible and wearable energy storage devices.

Received 12th October 2018
Accepted 19th November 2018

DOI: 10.1039/c8ra08403c

rsc.li/rsc-advances

Introduction

The emergence of portable and wearable electronics has promoted urgent research on appropriate flexible power supply devices with lightweight, high stability, and good electrochemical performances.[1–4] In recent years, considerable efforts have been devoted to developing wearable SCs and LIBs (lithium-ion batteries).[5–8] In particular, SCs, accompanied by the low-cost manufacturing process, store energy through ion adsorption or redox reaction.[9,10] SCs can be safely and quickly charged/discharged, exhibit high power density, long cycle life, and environmental friendliness, which are considered as one of the most promising energy storage devices.[9,10] The textile-based SCs fabricated by electrochemical deposition, chemical polymerization or facile dipping-drying methods, have been widely studied due to their high mechanical strength and electrical conductivity.[11–15] Textiles, with flexibility and porosity properties, can be integrated into smart garments for powering wearable electronics. The active materials used in the electrodes of textile SCs have mainly focused on carbon and carbon derivatives (graphene, carbon nanotubes, active carbon *et al.*), conducting polymers (polypyrrole and polyaniline), and transition metal oxides (MnO_2).[11–15] So far, a series of achievements based on textile-based SCs have been obtained.[11–15] For example, Cui *et al.* respectively developed CNTs and graphene-based stretchable and conductive energy textiles, which displayed high capacitance, excellent cycling performance, and mechanical properties.[11,12] However, most reported textile-based SCs are difficult to have both simple manufacturing techniques and high capacitance performance. So, in order to improve the capacitive performance and reduce the cost, it is necessary to prepare other textile electrodes based on new active materials.

Recently, MXenes, a new family of two-dimensional (2D) transition metal carbides or nitrides, have shown great promise as potential materials for electrochemical energy storage due to their great conductivity (up to 9880 S cm^{-1}), well hydrophilicity, and excellent ion intercalation behavior.[16–25] In general, MXenes with a formula of $M_{n+1}X_nT_x$ where M is a transition metal, X is carbon (C) and/or nitrogen (N), T_x represents the surface termination groups such as F, O, and OH, have been prepared by selectively etching the A layers from their ternary carbide or nitride precursors, MAX phases.[25,26] Until now, more than 20 MXenes were fabricated by the wet chemical etching methods.[25] Among them, $Ti_3C_2T_x$ is earliest and most deeply investigated MXene, which is widely applied in the energy storage,[16–19]

School of Sciences, Hubei University of Automotive Technology, Shiyan 442002, P. R. China. E-mail: mayn@huat.edu.cn

† Electronic supplementary information (ESI) available: Fig. S1–S8. See DOI: 10.1039/c8ra08403c

electromagnetic shielding,[27,28] molecular sieving membranes,[29] force sensors[30,31] and so on. $Ti_3C_2T_x$ nanosheets display large-area surface, rich physical and chemical properties and good conductivity, which is ideal for constructing low-cost and high-performance SCs.

Actually, $Ti_3C_2T_x$ MXene has already been proved an excellent electrode material used in typically sandwiched structure SCs,[20] fiber SCs[32,33] and interdigitated coplanar micro-supercapacitors.[34,35] For example, Michael Ghidiu *et al.* reported the $Ti_3C_2T_x$ 'clay' films with volumetric capacitances of up to 900 F cm^{-3}, which is far higher than that of carbon materials.[23] And Xu *et al.* reported the $Ti_3C_2T_x$-based asymmetrical micro-supercapacitors fabricated by the screen-printing method, which possesses high energy density (8.84 μW h cm^{-2}) and can drive the force sensor to detect the applied pressure variation.[36] To further improve high-rate performance and ion accessibility to active sites of $Ti_3C_2T_x$ MXene, much works have been made to construct MXene electrode architectures.[16,37,38] For instance, the vertical alignment of MXene nanosheets were achieved by mechanical shearing of a discotic lamellar liquid-crystal phase of $Ti_3C_2T_x$, which not only can effectively improve ion transport, but also is independent of film thickness.[38] Although the research of $Ti_3C_2T_x$-based SCs has made a series of breakthroughs, their preparation technique need further optimization for the sake of commercialization (mainly for low-cost and simple preparation) and stability. On the other hand, during the using process, it is necessary for $Ti_3C_2T_x$ MXene to avoid its restack and oxidization which will hinder the relative capacitance and stability.

Herein, a lightweight, flexible polypyrrole–MXene based SCs is developed by combining the good electrochemical performance of $Ti_3C_2T_x$ with the porous and hydrophilic characteristics of cotton textile. In detail, the MXene-based textile electrodes were fabricated by coating $Ti_3C_2T_x$ nanosheets on the surface of textile in the simple dipping–drying method. To improve the capacitive performance of the MXene-based textile electrode and meanwhile avoid the poor oxygen oxidation of MXene, PPy, a kind of pseudocapacitance materials (theoretical specific capacitance is up to 620 F g^{-1})[39–41] was electrochemically deposited on the surface of MXene textiles, which formed the MXene–PPy textile electrode. Finally, a symmetrical solid-state supercapacitor based on MXene–PPy textile was fabricated by means of macroporous textiles as the separators. The SCs based on the MXene–PPy textile reveals good capacitance performance and flexibility, which will benefit the development of wearable electronics.

Result and discussion

Fig. 1 shows the schematic diagrams of PPy–MXene coated textile SCs. Textile fabric has a hierarchical, porous structure with rich hydrophilic groups such as hydroxyl groups, which allows the textile to absorb water and swell in MXene colloidal solution. Thus, the $Ti_3C_2T_x$ nanosheets with good hydrophilicity and metallic conductivity can uniformly coat onto the surface of the textile *via* a facile dipping-coating method. To further enhance the capacitive performance of the MXene-based textile

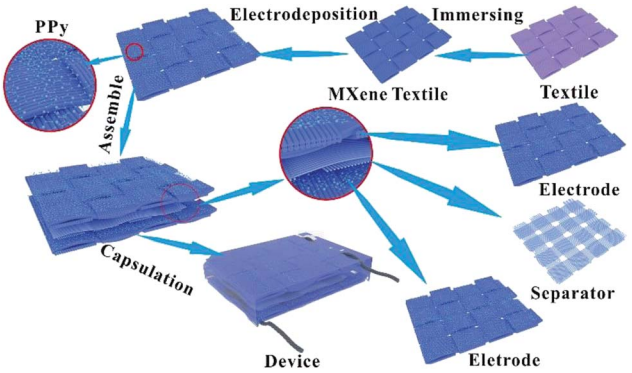

Fig. 1 Schematic diagrams of PPy–MXene coated textile SCs.

and meanwhile avoid oxidation of the exposed $Ti_3C_2T_x$, the pseudocapacitance material, PPy with good stability in ambient conditions[40] was electrochemically deposited onto the surface of the MXene-based textile. And the symmetrical solid-state SCs were synthesized by sandwiching macroporous textiles (as the separator) between two PPy–MXene coated textiles, where the H_2SO_4/PVA gel used the electrolyte. And a thin PE (polyethylene) film was fixed and packaged over the above SCs to prevent its complete dehydration.

The $Ti_3C_2T_x$ nanosheets were synthesized by selectively etching out the Al layer from the precursor Ti_3AlC_2 by HCl + LiF solution (Fig. S1†). The ternary Ti_3AlC_2 exhibits layered characteristic as shown in the SEM images (Fig. S2†). And the X-ray diffraction (XRD) The $Ti_3C_2T_x$ nanosheets are excellent lamellar structure, diverse lateral size and good transparency like the substrate as shown in the typical TEM image of Fig. 2a. From the electron diffraction (SAED) pattern in the inset of Fig. 2a, it is found that MXene $Ti_3C_2T_x$ nanosheets have a hexagonal crystal structure. It is known that the MXene nanosheets prepared by the solution method were terminated by the functional group such as hydroxyl and fluorine, which resulted in its uniform coating of the nanosheet onto the surface of the textile. From the SEM images of the MXene-based textile, the nanosheets tightly wrapped around the whole textile (Fig. S3c†), even each fiber that made up the textile, as shown in Fig. 2b and c. The MXene-based textile also shows excellent stretchable and flexible properties (Fig. S3†). In the presence of water and oxygen, the partial edge of $Ti_3C_2T_x$ nanosheet will oxidize into TiO_2,[42] which significantly affects the electrical conductivity, then decrease the electrochemical performance. To solve this problem, the PPy was electroplated onto the surface of MXene to prevent MXene's direct contact with water and oxygen. After the deposition, the PPy also firmly coated the MXene layer, forming the wrinkle, as shown in Fig. 2d and e. In addition, the X-ray diffraction (XRD) patterns were also investigated the MXene-based and PPy–MXene coated textile electrodes in Fig. 2f and S4.† It is revealed that the (002) peak at ~6° ascribed to $Ti_3C_2T_x$ appeared and the peak at ~39° attributed to Ti_3AlC_2 disappeared, meaning the successful preparation of MXene.[23] And the other peaks of the MXene-based textile are consistent with XRD patterns of the cellulose.[43] Moreover, after the PPy coating onto the surface MXene-based textile, the (002) peak of $Ti_3C_2T_x$

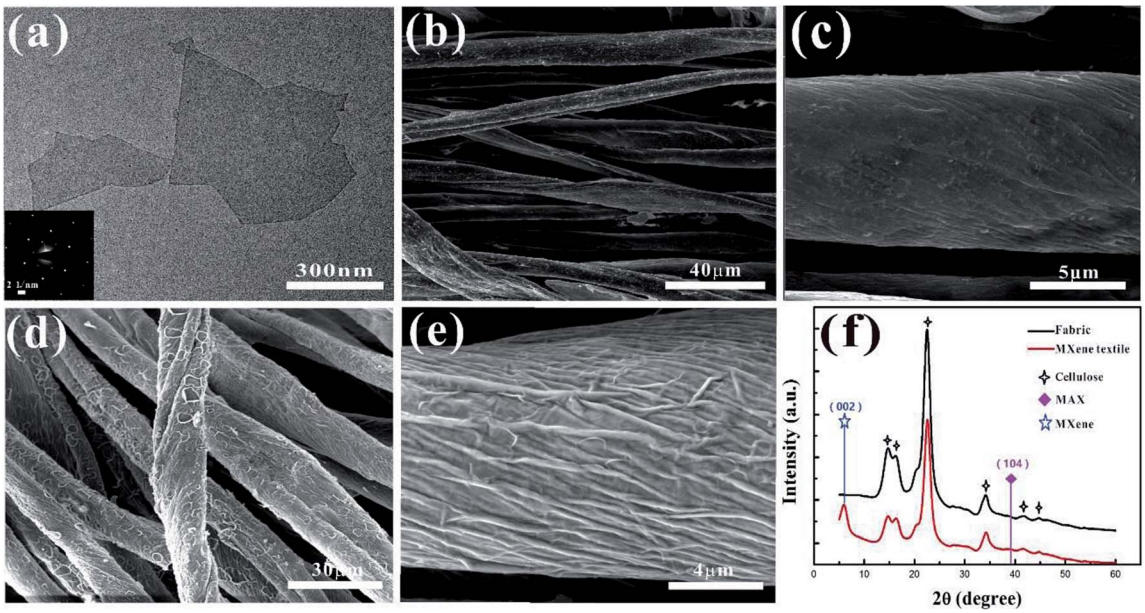

Fig. 2 Characterization of the MXene-based and PPy–MXene coated textile electrodes. (a) TEM image of $Ti_3C_2T_x$ nanosheet, the inset shows its corresponding diffraction pattern. (b) The represent SEM image of MXene-based textile. (c) The magnified SEM image of (b). (d) The represent SEM image of PPy–MXene coated textile. (e) The magnified SEM image of (d). (f) XRD patterns of the MXene-based and PPy–MXene coated textile.

disappeared, and the peaks of cellulose become weaken. And the Raman spectrum was measured to prove the existence of PPy (Fig. S5†). The band located at 1367 cm^{-1} is ascribed to ring stretching mode of PPy, and the band located at 1573 cm^{-1} is assigned to the conjugated structure of PPy.[44]

The three-electrode configuration was used for the electrochemical measurements to evaluate the performance of the MXene-based and PPy–MXene coated textile electrodes. To optimize the electrochemical performance of MXene-based textile, different soaking times of MXene colloidal solution for textile were carried out. It is found that to a certain extent, with the increase of the soaking times the performance of the MXene-based textile continuously increase (Fig. 3a), which attributes to the increase of active materials. But after the fourth times of MXene solution, the performance of the electrode tends to slightly decrease in Fig. 3a. This is because both the loading of active material and conductivity of electrodes approaches saturation after fourth soaking in Fig. S3.† On the other hand, the excess active materials on the surface of textile emerge the stack between the MXene nanosheets, leading to the degradation of performance. And the galvanostatic charge–discharge (GCD) curves (Fig. 3b) of the MXene-based textile were consistent with the CV curves, indicating after the 4 soaking times in MXene solution, the electrochemical performance is the maximum.

The electrochemical performance of the MXene-based electrode with 4 times soaking was systematically studied by CV and GCD measurements. Fig. 3c presents the CV curves of the MXene-based textile with scanning rates from 5 to 100 mV s^{-1}. As expected, the MXene-based textile electrode exhibited well capacitive performance with similar rectangular CV curves. And the GCD measurements of the MXene-based textile show good linear potential–time, demonstrating a good capacitance performance of the electrode in Fig. 3d. In addition, Fig. 3e and f display the specific capacitance evaluated from the above CV and GCD results. The specific capacitances were as high as 182.7 F g^{-1} (scan rate of 10 mV s^{-1}) and 105.6 F g^{-1} (current density of 0.9 mA cm^{-2}), which is higher than carbon nanotube (CNT) and active carbon reported.[11,13]

To further improve the capacitance performance of the MXene-based electrode and avoid the oxidation of the MXene, PPy was electrochemically deposited onto the surface of the MXene-based textile. The CV and GCD curves confirmed that after coating PPy, the capacitance performance of the MXene-based electrode was significantly enhanced, as shown in Fig. 4a–c. By comparing CV curves of different deposition times of PPy at a scan rate of 50 mV s^{-1}, the deposition 4 min PPy will greatly improve the capacitance performance of the MXene-based electrode (Fig. S6†). And the enclosed area of the CV curve from PPy–MXene coated textile electrode was about 3 times larger than that from the MXene-based electrode, where the specific capacitance of PPy–MXene coated textile electrode was up to 343.2 F g^{-1} as shown in Fig. 4c. Fig. 4d–f exhibited the detailed CV and GCD curves. It is found the CV curves have a good symmetrical rectangular shape and large enclosed area at a scan rate in the range of 5–100 mV s^{-1}. And the GCD curves show the shape of an isosceles triangle. The calculated capacitance from GCD curves was as high as 275.2 F g^{-1} (current density of 1.0 A cm^{-2}).

The symmetry SCs based on the PPy–MXene coated textile were assembled by using H_2SO_4/PVA as a solid electrolyte, the porous textile as the separator. The SCs based on PPy–MXene coated textile have a stable potential window of to 0.6 V, as shown in Fig. 5. The symmetrical rectangular shape and

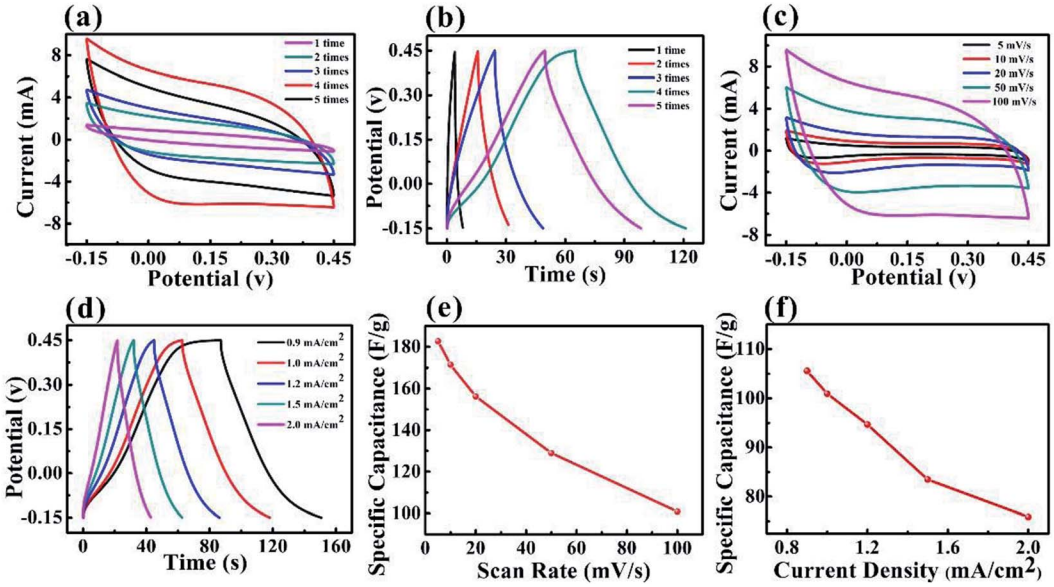

Fig. 3 Electrochemical performance of the MXene-based textile electrode. (a) CV curves of the MXene-based textile electrode with different soak times. (b) GCD curves of the MXene-based textile electrode with different soak times. (c) CV curves of the MXene-based textile electrode with soaking 4 times at different scan rate. (d) GCD curves of the MXene-based textile electrode with soaking 4 times at various current densities. (e) The relation of specific capacitance and scan rate. (f) The specific capacitance at different current density.

enclosed areas in the CV curves at scan rates from 5 up to 100 mV s^{-1} in Fig. 5a, and linear plots of the GCD curves at different current densities varying from 0.5 to 2.5 mA cm^{-2} in Fig. 5b, indicated the excellent performance of the SCs. In addition, the Nyquist curve of SC in Fig. 5c displayed distinct semicircle shape and good conductivity. Fig. 5d shows the Ragone plot of energy density *versus* power density values considering the total mass of active materials from electrodes. At a current density of 0.5 mA cm^{-2}, the SCs based on PPy–MXene coated textile has an energy density of 1.30 mW h g^{-1} and a power density of 41.1 mW g^{-1}. And when the current density is 2.5 mA cm^{-1-2}, the energy density is reduced to 0.42 mW h g^{-1} and the power density is as high 205.48 mW g^{-1}. And the cyclic performances of symmetrical solid-state supercapacitor based on MXene–PPy textile is measured in Fig. S7.† In practical application, SCs often need to provide different voltages or currents. So it is required to connect supercapacitors in series or in parallel. Fig. 5e shows the CV curves of the SCs

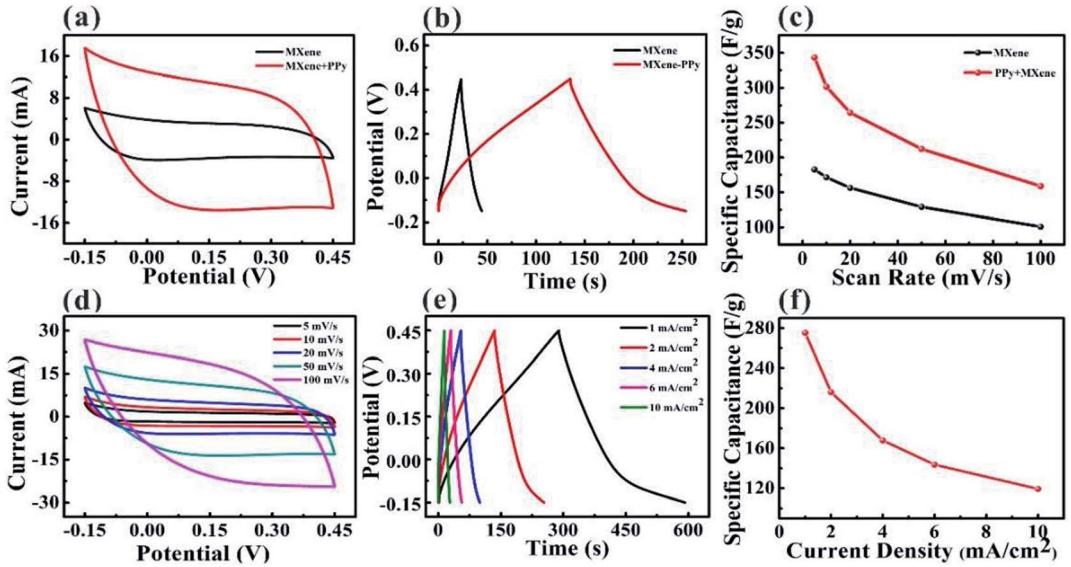

Fig. 4 Electrochemical performance of PPy–MXene coated the textile electrode. (a) The comparison of CV curves between MXene-based and PPy–MXene coated textile electrode at a scan rate of 50 mV s^{-1}. (b) The comparison of GCD curves between MXene-based and PPy–MXene coated textile electrode under a current density of 2 mA cm^{-2}. (c) The comparison of specific capacitance between MXene-based and PPy–MXene coated textile electrode. (d) CV curves of PPy–MXene coated textile electrode at the different scan rate. (e) GCD curves of PPy–MXene coated textile electrode at various current densities. (f) The specific capacitance of PPy–MXene coated textile electrode with respect to scan rate.

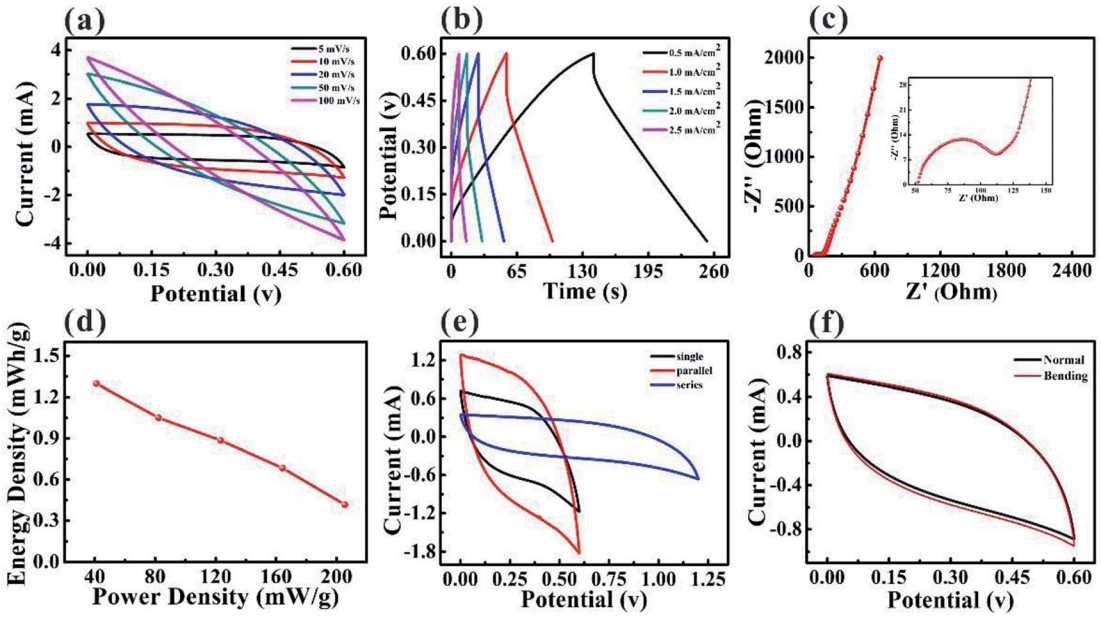

Fig. 5 Electrochemical performance of symmetrical solid-state supercapacitor based on MXene–PPy textile. (a) CV curves of PPy–MXene coated textile supercapacitor at the different scan rate. (b) GCD curves PPy–MXene coated textile supercapacitor at various current densities. (c) Nyquist plot of the PPy–MXene coated textile supercapacitor. (d) Energy and power density plot of PPy–MXene coated textile supercapacitor. (e) CV curves of a single and two SCs connected in series and parallel. (f) CV curves of the PPy–MXene coated textile supercapacitor in the normal and bending states.

based on PPy–MXene coated textile in series and in parallel with a scan rate of 10 mV s^{-1}. The capacitance after the series connection is half that of a single capacitor, while capacitance after parallel connection is twice that of a single one. And the MXene-based textile supercapacitors in series can lighten the LED bulb (Fig. S8†). In order to study the flexibility of SCs based on PPy–MXene coated textile, its CV curves under normal and bending state at a scan rate of 10 mV s^{-1} were measured as shown in Fig. 5f. It is found that the two CV curves are almost coincident, indicating its good flexibility.

Conclusions

In summary, a kind of smart and flexible SCs based on MXene have been fabricated by using a simple and scalable "dipping and drying" method. The capacitance of MXene-based textile progressively increases with the mass loading of the active material in a certain amount. And after the 4th times soaking of MXene solution (2 mg ml^{-1}), the electrochemical performance of MXene-based electrode achieve optimal value (182.70 F g^{-1}). To improve the capacitive performance of the MXene-based electrode and avoid the poor oxygen oxidation of $Ti_3C_2T_x$, we electrochemically deposited PPy onto the surface of MXene textiles, which achieve a high specific capacitance (343.20 F g^{-1}). And the symmetrical solid-state SCs based on MXene–PPy textiles device also show well electrochemical performance and flexibility. Our strategy not only supports an important way to design SCs, but also extends MXenes to other energy conversion and storage devices besides supercapacitors.

Experimental section

Materials

TiH_2 (99 wt% ~325 mesh), Al (99.9 wt% ~300 mesh), and C powders (99 wt% ~200 mesh) were purchased from Aladdin Reagent Company. The HCl and LiF were purchased from the Sinopharm Chemical Reagent Company. Milli-Q water (18.2 MΩ, resistivity) was used for all solution preparations.

Preparation of $Ti_3C_2T_x$ MXene nanosheet

The Ti_3AlC_2 MAX phase was synthesized in the high-temperature solid phase method, where TiH_2, Al, and C powders were mixed in a molar ratio of 3 : 1.1 : 2, then reacted for 2 h at 1400 °C. $Ti_3C_2T_x$ MXene nanosheets were prepared following the MILD method by selective etching Al layer from Ti_3AlC_2 using wet chemical etching method.[27] The specific steps are processed by firstly adding 1 g LiF added into 20 ml 9 M HCl, followed by stirring 10 min. Then 1 g Ti_3AlC_2 powder was slowly added to the above mixing solution and reacted for 24 h at 35 °C. Finally, the acidic suspension was centrifuged under 3500 rpm for several times, until a stable dark green supernatant of $Ti_3C_2T_x$ was observed with pH ≥ 6. The $Ti_3C_2T_x$ nanosheets were then finally obtained by sonicated in a cold bath for 50 min and followed by centrifugation at 3500 rpm for 60 min.

Preparation of MXene-based textile electrode

The plain cotton textiles were washed with acetone, ethanol and deionized water for 30 minutes, followed dried. The above clean textile was cut to appropriate size, then immersed in 2 mg ml^{-1}

MXene solution (which was diluted by the above MXene stock solution) for several times ranging from one to five. The MXene-coated textile was dried in the vacuum oven at 60 °C, thus avoiding the oxidation of MXene.

Preparation of PPy–MXene coated the textile electrode

The PPy–MXene coated textile electrode was prepared by the electrochemical deposition, where the electrolyte solution consisted of $NaClO_4$ (0.2 M) and pyrrole (5%). PPy was electroplated onto the surface of MXene-based textile *via* a three-electrode electroplating system, in which MXene-based textile electrode served as the working electrode, carbon was used as the counter electrode, and Ag/AgCl as the reference electrode. During electroplating, the voltage was set at 0.8 V and the time is ranging from 1 min to 4 min. The resultant MXene–PPy textile was obtained by rinsing with DI water, and then vacuum drying at 50 °C.

Assembly of solid-state MXene–PPy textile SCs

The MXene–PPy textile electrodes were cut into 1 × 2 cm to fabricate the symmetrical solid-state SCs. H_2SO_4/PVA was used as the solid electrolyte, the macroporous textiles as the separators, the hydrophobic conductive carbon fiber as the current collector which prevent the occurrence of the electric capillary.

Characterization

The morphology, structure, and composition of MAX, MXene and electrodes were investigated by high-resolution field emission scanning electron microscopy (SEM, FEI Nova NanoSEM 450, 10 kV), transmission electron microscopy (TEM, FEI Titan G260-300) and a X-ray diffractometer (XRD Rigaku X-ray diffractometer with Cu Kα-radiation and Ni filter). Raman spectroscopy was recorded by a Renishaw inVia Raman spectrometer with 532 nm laser light. Electrochemical tests including CV (Cyclic Voltammograms), GCD (Galvanostatic Charge–Discharge), and EIS (Electrochemical Impedance Spectroscopy) were measured by using an electrochemical workstation (CHI 660E). To test the electrochemical performance of the MXene-based and MXene–PPy textile electrodes, a three-electrode system was used with a 1 M H_2SO_4 solution, a carbon electrode and an Ag/AgCl electrode respectively as the electrolyte, counter electrode, and reference electrode. Electrochemical measurements of the symmetrical solid-state SCs were measured in a two-electrode cell at room temperature in H_2SO_4–PVA solid electrolyte.

Conflicts of interest

There are no conflicts to declare.

Acknowledgements

This work was supported by Key Laboratory of Automotive Power Train and Electronics (Hubei University of Automotive Technology), the Natural Science Foundation of Hubei Province (No. 2014CFB631), the Foundation of Hubei Educational Committee (No. Q20141802) and Doctoral Research Fund of HUAT.

Notes and references

1 C. Choi, H. J. Sim, G. M. Spinks, G. M. Lepró, X. Baughman, R. H. Baughman and S. J. Kim, *Adv. Energy Mater.*, 2016, **6**, 1502119.
2 Q. Huang, D. Wang and Z. Zheng, *Adv. Energy Mater.*, 2016, **6**, 1600783.
3 K. Jost, D. P. Durkin, L. M. Haverhals, E. K. Brown, M. Langenstein, H. C. De Long, P. C. Trulove, Y. Gogotsi and G. Dion, *Adv. Energy Mater.*, 2015, **5**, 1401286.
4 B. C. Kim, J. Y. Hong, G. G. Wallace and H. S. Park, *Adv. Energy Mater.*, 2015, **5**, 1500959.
5 J. Janek and W. G. Zeier, *Nat. Energy*, 2016, **1**, 16141.
6 G. Zhou, F. Li and H. M. Cheng, *Energy Environ. Sci.*, 2014, **7**, 1307–1338.
7 W. Liu, M. S. Song, B. Kong and Y. Cui, *Adv. Mater.*, 2017, **29**, 1603436.
8 Y. Huang, H. Li, Z. Wang, M. Zhu, Z. Pei, Q. Xue, Y. Huang and C. Zhi, *Nano Energy*, 2016, **22**, 422–438.
9 Y. Huang, M. S. Zhu, Y. Huang, Z. X. Pei, H. F. Li, Z. F. Wang, Q. Xue and C. Y. Zhi, *Adv. Mater.*, 2016, **28**, 8344–8364.
10 Y. L. Shao, M. F. El-Kady, L. J. Wang, Q. H. Zhang, Y. G. Li, H. Z. Wang, M. F. Mousavi and R. B. Kaner, *Chem. Soc. Rev.*, 2015, **44**, 3639–3665.
11 L. Hu, M. Pasta, F. L. Mantia, L. Cui, S. Jeong, H. D. Deshazer, J. W. Choi, S. M. Han and Y. Cui, *Nano Lett.*, 2010, **10**, 708–714.
12 G. Yu, L. Hu, M. Vosgueritchian, H. Wang, X. Xie, J. R. McDonough, X. Cui, Y. Cui and Z. Bao, *Nano Lett.*, 2011, **11**, 2905–2911.
13 K. Jost, C. R. Perez, J. K. McDonough, V. Presser, M. Heon, G. Dion and Y. Gogotsi, *Energy Environ. Sci.*, 2011, **4**, 5060–5067.
14 X. Chen, H. Lin, P. Chen, G. Guan, J. Deng and H. Peng, *Adv. Mater.*, 2014, **26**, 4444–4449.
15 T. G. Yun, B. I. Hwang, D. Kim, S. Hyun and S. M. Han, *ACS Appl. Mater. Interfaces*, 2015, **7**, 9228–9234.
16 M. R. Lukatskaya, S. Kota, Z. Lin, M. Zhao, N. Shpigel, M. D. Levi, J. Halim, P. Taberna, M. W. Barsoum, P. Simon and Y. Gogotsi, *Nat. Energy*, 2017, **17105**, 1–6.
17 J. C. Lei, X. Zhang and Z. Zhou, *Front. Phys.*, 2015, **10**, 276–286.
18 X. Zhang, Z. Zhang and Z. Zhou, *J. Energy Chem.*, 2018, **27**, 73–85.
19 M. Hu, Z. Li, H. Zhang, T. Hu, C. Zhang, Z. Wu and X. Wang, *Chem. Commun.*, 2015, **51**, 13531–13533.
20 C. J. Zhang, B. Anasori, A. Seral-Ascaso, S. H. Park, N. McEvoy, A. Shmeliov, G. S. Duesberg, J. N. Coleman, Y. Gogots and V. Nicolosi, *Adv. Mater.*, 2017, **29**, 1702678.
21 M. R. Lukatskaya, O. Mashtalir, C. E. Ren, Y. Dall'Agnese, P. Rozier, P. L. Taberna, M. Naguib, P. Simon, M. W. Barsoum and Y. Gogotsi, *Science*, 2013, **341**, 1502–1505.

22 O. Mashtalir, M. Naguib, V. N. Mochalin, Y. Dall'Agnese, M. Heon, M. W. Barsoum and Y. Gogotsi, *Nat. Commun.*, 2013, **4**, 1716.
23 M. Ghidiu, M. R. Lukatskaya, M. Q. Zhao, Y. Gogotsi and M. W. Barsoum, *Nature*, 2014, **516**, 78–81.
24 M. Naguib, V. N. Mochalin, M. W. Barsoum and Y. Gogotsi, *Adv. Mater.*, 2014, **26**, 992–1005.
25 B. Anasori, M. R. Lukatskaya and Y. Gogotsi, *Nat. Rev. Mater.*, 2017, **2**, 16098.
26 M. Naguib, V. N. Mochalin, M. W. Barsoum and Y. Gogotsi, *Adv. Mater.*, 2014, **26**, 992–1005.
27 F. Shahzad, M. Alhabeb, C. B. Hatter, B. Anasori, S. M. Hong, C. M. Koo and Y. Gogotsi, *Science*, 2016, **353**, 1137–1140.
28 J. Liu, H. B. Zhang, R. Sun, Y. Liu, Z. Liu, A. Zhou and Z. Z. Yu, *Adv. Mater.*, 2017, **29**, 1702367.
29 L. Ding, Y. Wei, L. Li, T. Zhang, H. Wang, J. Xue, L.-X. Ding, S. Wang, J. Caro and Y. Gogotsi, *Nat. Commun.*, 2018, **9**, 155.
30 Y. Ma, Y. Yue, H. Zhang, F. Cheng, W. Zhao, J. Rao, S. Luo, J. Wang, X. Jiang, Z. Liu, N. Liu and Y. Gao, *ACS Nano*, 2018, **12**, 3209–3216.
31 Y. Yue, N. Liu, W. Liu, M. Li, Y. Ma, C. Luo, S. Wang, J. Rao, X. Hu, J. Su, Z. Zhang, Q. Huang, Y. Gao and Z. Zhang, *Nano Energy*, 2018, **50**, 79–87.
32 S. Seyedin, E. R. S. Yanza and J. M. Razal, *J. Mater. Chem. A*, 2017, **5**, 24076–24082.
33 M. Hu, Z. Li, G. Li, T. Hu, C. Zhang and X. Wang, *Adv. Mater. Technol.*, 2017, **2**, 1700143.
34 Y. Y. Peng, B. Akuzum, N. Kurra, M. Q. Zhao, M. Alhabeb, B. Anasori, E. C. Kumbur, H. N. Alshareef, M. –D. Ger and Y. Gogotsi, *Energy Environ. Sci.*, 2016, **9**, 2847–2854.
35 N. Kurra, B. Ahmed, Y. Gogotsi and H. N. Alshareef, *Adv. Energy Mater.*, 2016, **6**, 1601372.
36 S. Xu, Y. Dall'Agnese, G. Wei, C. Zhang, Y. Gogotsi and W. Han, *Nano Energy*, 2018, **50**, 479–488.
37 J. Yan, C. E. Ren, K. Maleski, C. B. Hatter, B. Anasori, P. Urbankowski, A. Sarycheva and Y. Gogotsi, *Adv. Funct. Mater.*, 2017, **27**, 1701264.
38 Y. Xia, T. S. Mathis, M. Q. Zhao, B. Anasori, A. Dang, Z. Zhou, H. Cho, Y. Gogotsi and S. Yang, *Nature*, 2018, **557**, 409–412.
39 Y. Yue, Z. Yang, N. Liu, W. Liu, H. Zhang, Y. Ma, C. Yang, J. Su, L. Li, F. Long, Z. Zou and Y. Gao, *ACS Nano*, 2016, **10**, 11249–11257.
40 J. H. Kim, A. K. Sharma and Y. S. Lee, *Mater. Lett.*, 2006, **60**, 1697–1701.
41 K. Lota, V. Khomenko and E. Frackowiak, *J. Phys. Chem. Solids*, 2004, **65**, 295–301.
42 C. J. Zhang, S. Pinilla, N. McEvoy, C. P. Cullen, B. Anasori, E. Long, A. Seral-Ascaso, A. Shmeliov, D. Krishnan, C. Morant, X. Liu, G. S. Duesberg, Y. Gogotsi and V. Nicolosi, *Chem. Mater.*, 2017, **29**, 4848–4856.
43 H. Zhao, J. H. Kwak, Z. C. Zhang, H. M. Brown, B. W. Arey and J. E. Holladay, *Carbohydr. Polym.*, 2007, **68**, 235–241.
44 C. Luo, N. Liu, H. Zhang, W. Liu, Y. Yue, S. Wang, J. Rao, C. Yang, J. Su, X. Jiang and Y. Gao, *Nano Energy*, 2017, **41**, 527–534.